Tri-Level Scheduling Model Considering Residential Demand Flexibility of Aggregated HVACs and EVs Under Distribution LMP

Xiaofei Wang, *Graduate Student Member, IEEE*, Fangxing Li, *Fellow, IEEE*, Jin Dong, *Member, IEEE*, Mohammed M. Olama, *Senior Member, IEEE*, Qiwei Zhang, *Graduate Student Member, IEEE*, Qingxin Shi, *Member, IEEE*, Byungkwon Park, *Member, IEEE*, and Teja Kuruganti, *Senior Member, IEEE*

***Abstract*—Residential loads, especially heating, ventilation and air conditioners (HVACs) and electric vehicles (EVs), have great potentials to provide demand flexibility which is an attribute of grid-interactive efficient buildings (GEB). Under this new paradigm, EV and HVAC aggregator models are first developed in this paper to represent the fleet of GEBs, in which the aggregated parameters are obtained based on a new approach of data generation and least squares parameter estimation (DG-LSPE), which can deal with heterogeneous HVACs. Then, a tri-level bidding and dispatching framework is established based on competitive distribution operation with distribution locational marginal price (DLMP). The first two levels form a bilevel model to optimize the aggregators' payment and to represent the interdependency between load aggregators and the distribution system operator (DSO) using DLMP, and the third level is to dispatch the optimal load aggregation to all residents by the proposed priority list-based demand dispatching algorithm. Finally, case studies on a modified IEEE 33-Bus system illustrate three main technical reasons of payment reduction due to demand flexibility: load shifts, DLMP step changes, and power losses. They can be used as general guidelines for better decision-making for future planning and operation of demand response programs.**

***Index Terms*—EV aggregator, HVAC aggregator, distribution locational marginal price (DLMP), residential demand flexibility, tri-level scheduling model, load shift, DLMP step change.**

Manuscript received October 20, 2020; revised March 16, 2021; accepted April 17, 2021. Date of publication May 28, 2021; date of current version August 23, 2021. This work was supported in part by the U.S. Department of Energy (DOE), including DOE's Grid Modernization Laboratory Consortium (GMLC), Office of Electricity, and Building Technologies Office, and in part by the CURENT which is an Engineering Research Center funded by the U.S. National Science Foundation (NSF) and DOE under NSF Award EEC-1041877. Paper no. TSG-01569-2020. *(Corresponding author: Fangxing Li.)*

Xiaofei Wang, Fangxing Li, Qiwei Zhang, and Qingxin Shi are with the Department of Electrical Engineering and Computer Sciences, University of Tennessee, Knoxville, TN 37996 USA (e-mail: xwang158@vols.utk.edu; fli6@utk.edu; qzhang41@vols.utk.edu; qshi1@vols.utk.edu).

Jin Dong is with the Electrification and Energy Infrastructures Division, Oak Ridge National Laboratory, Oak Ridge, TN 37831 USA (e-mail: dongj@ornl.gov).

Mohammed M. Olama, Byungkwon Park, and Teja Kuruganti are with the Computational Sciences and Engineering Division, Oak Ridge National Laboratory, Oak Ridge, TN 37831 USA (e-mail: olamahussemm@ornl.gov; parkb@ornl.gov; kurugantipv@ornl.gov).

Color versions of one or more figures in this article are available at https://doi.org/10.1109/TSG.2021.3075386.

Digital Object Identifier 10.1109/TSG.2021.3075386

NOMENCLATURE

Sets

T	Set of time slots
H	Set of HVAC aggregators
E	Set of EV aggregators
G	Set of all generators
B	Set of all nodes
S	Substation.

Constants

$P_{i,t}^{MT,min}$/ $P_{i,t}^{MT,max}$	Minimum/maximum active power of MT i at time t
α_i	Power factor of DG i
$P_{i,t}^{PV,fore}$	Forecasted active power of PV i at time t
$Q_{i,t}^{SVC,min}$/ $Q_{i,t}^{SVC,max}$	Minimum/maximum reactive power of SVC i at time t
η^C, η^D	Charge/discharge efficiency of EV
$P_{i,t}^{C,max}$/ $P_{i,t}^{Dis,max}$	Maximum charge/discharge power of EV aggregator i at time t
$SOC_i^{E,min}$	Minimum state of charge of EV aggregator i
$SOC_i^{E,max}$	Maximum state of charge of EV aggregator i
E_i^R	Rated energy capacity of EV aggregator i
N_i^e	Number of EVs participating in aggregator i
N_i^{piles}	Number of charging piles in charging station i
p_j^C	Rated charging power of EV j
E_j^{rated}	Rated energy of EV j
e_j^d	Driving energy consumption of EV j per mile
d_j	Driving distance over a day
a_j, b_j, g_j	Coefficients of the thermal function of HVAC j
θ_{out}	Day-ahead forecasted outdoor temperature
$\theta^{min}/\theta^{max}$	Comfortable temperature boundary
R_j, C_j	Thermal resistance and capacitance of HVAC j
η^H	Cooling efficiency of HVAC
P^{rated}	Rated power of HVAC
$\tilde{a}_i$,$\tilde{b}_i$,$\tilde{g}_i$	Coefficients of the thermal transfer function of HVAC aggregator i
N_i^h	Number of HVACs participating in aggregator i
syn_i^{min}/	Minimum/maximum synchronicity rate of

syn_i^{max}	HVAC aggregator i
$\Delta u_i^{dr}/\Delta u_i^{ur}$	Ramp down/up rate of HVAC aggregator i
$SOC_i^{H,min}$	Minimum state of charge of HVAC aggregator i
$SOC_i^{H,max}$	Maximum state of charge of HVAC aggregator i
$\sigma_{S,t}^p/\sigma_{S,t}^q$	Active/reactive LMP at the substation at time t
$\sigma_{i,t}^p/\sigma_{i,t}^q$	Active/reactive bidding price of generator i at time t
$P_{i,t}^D/Q_{i,t}^D$	Fixed active/reactive load demand of node i at time t
V^{min}/V^{max}	Minimum/maximum voltage constraints.

Variables

P_t^S/Q_t^S	Active/reactive power drawn from the wholesale market at time t
$P_{i,t}^{MT}/Q_{i,t}^{MT}$	Active/reactive power of MT i at time t
$P_{i,t}^{PV}/Q_{i,t}^{PV}$	Active/reactive power of PV i at time t
$Q_{i,t}^{SVC}$	Reactive power of SVC i at time t
$E_{i,t}$	Energy of EV aggregator i at time t
$P_{i,t}^C/P_{i,t}^{Dis}$	Charge/discharge power of EV aggregator i at time t
$\theta_{j,t}$	Indoor temperature of building j at time t
$u_{j,t}$	Binary variable stating the ON/OFF of HVAC j at time t
$\tilde{\theta}_{i,t}$	Equivalent indoor temperature of HVAC aggregator i at time t
$\tilde{u}_{i,t}$	ON-state ratio of HVACs in aggregator i at time t
$P_{i,t}^H$	Active power of HVAC aggregator i at time t
$SOC_{i,t}$	State of charge of HVAC aggregator i at time t
$\pi_{i,t}^p$	Active DLMP of node i at time t
P_t^{loss}/Q_t^{loss}	Active/reactive power loss at time t
$V_{j,t}$	Voltage of node j at time t
$\pi_{i,t}^p$	Active DLMP at node i at time t
λ_t^p/λ_t^q	Lagrangian multipliers associated with active/reactive power balance constraints
$\omega_{i,t}^{(.),min}$, $\omega_{i,t}^{(.),max}$	Lagrangian multipliers associated with the voltage constraints, and the power output limits
$\kappa_{i,t}^-$,$\kappa_{i,t}^+$	Lagrangian multipliers associated with reactive power constraints.

I. Introduction

INSPIRED by the smart grid concept, at the generation side, the deployment of distributed generators (DGs), such as photovoltaic (PV), microturbine (MT) and wind turbine (WT), has been increasing in the past decades in distribution systems [1]. Meanwhile, at the load side, industrial and commercial customers are encouraged to participate in demand response (DR) programs. The proliferation of all these types of distributed energy resources (DERs) makes the distribution system more flexible and active [2]. Also, the advanced metering infrastructure like bilateral smart meter facilitates the information exchange between DERs and the distribution system operator (DSO) [3]. With this background, it is believed that DERs are driving the transition from a passive distribution system to a market-based one that aims to achieve the optimal allocation of all DERs [4].

In the transmission level market, locational marginal price (LMP) has been widely implemented by ISOs, such as PJM, New York ISO, ISO-New England, etc. [5]. In general, the LMP obtained by the DCOPF consists of energy and congestion components. However, congestion rarely occurs in the distribution network due to its radial topology. Furthermore, the high R/X ratio and voltage drop are typical characteristics of the distribution network, but the transmission-level LMP model does not include these components. All of these show that LMP is not appropriate in the distribution network. In the research community, some previous works are extending LMP to distribution locational marginal price (DLMP). In [6], DLMP is developed in a distribution system. In [7], [8], DSO determines DLMP based on generation offers and load bids by clearing the market. References [2] and [9] integrate the voltage component for DLMP and LMP, respectively. Reference [10] provides an interval prediction for the DLMP considering the uncertainty of renewables. All these works show that DLMP can reflect characteristics of operation and electricity pricing information in the distribution system. Thus, DLMP can be naturally considered as a price signal to incentivize consumers to adjust their loads to save electricity bills.

According to [11], heating, ventilation and air conditioners (HVACs) account for 45% of average summer peak-day loads. Also, the building's characteristic of thermal storage provides great demand flexibility by shedding and shifting HVAC load because the indoor temperature does not change fast due to thermal inertia [12], [13]. Together with electric vehicles (EVs) that have electricity storages, they are the ideal residential DR candidates to provide demand flexibility which is an attribute of grid-interactive efficient buildings (GEB).

Appropriate price signals can efficiently guide consumers to change their consumption patterns. This is beneficial to both consumers and the distribution system. Previous studies of the residential DR in response to price signals can be categorized into two groups based on the existence of the completely competitive distribution level market. 1) No such a market: time of use (TOU), critical peak pricing (CPP), peak time rebate (PTR), and real-time pricing (RTP) are the commonly used electricity rates. They are usually pre-determined and fixed [14]. In [15], the authors design a Smart Home Controller strategy to maximize customer economic saving with the adoption of TOU. The survey of a CPP experiment in California [16] shows a statistical response of residential loads to the CPP. Rational consumer behavior in a PTR mechanism is investigated in [17]. Reference [18] studies the optimal precooling of HVACs under time-varying electricity prices. Reference [19] proposes a dynamic DR control strategy to adjust the set-point temperature of HVACs according to RTP. Reference [20] presents an alternating direction method of multipliers (ADMM)-based residential DR management strategy. 2) With a completely competitive market: the work in [21] proposes an optimal bidding strategy for the load serving entity to profitably bid aggregated DR in the day ahead wholesale market. In [22], [23], DLMP is utilized to optimize the EV charging schedule to alleviate the congestion issue. In [24], [25], DLMP considering distribution congestion

price is proposed to guide the DR to prevent congestion. These studies show the effectiveness of DLMP in congestion management. However, the power losses are usually too high to be neglected due to the high R/X ratio, and the voltage is critical for the reliable operation of a distribution system. Thus, these factors should be considered in DLMP algorithms. In addition, compared with the broad DR concept, proper integration with the actual HVAC/EV models is highly necessary for industrial deployment. Also, as a participant in a competitive market, residential loads integrated at a large scale can affect DLMP. Thus, residents have the motivation to consume electricity strategically to minimize their electricity bills, possibly via an aggregator.

Based on these considerations, this paper focuses on reducing residents' electricity bills by proposing a novel tri-level model based on DLMP. The first level is to minimize residents' electricity payment by optimizing aggregated residential HVAC/EV schedules according to DLMP in the second level. The second level is to clear the day-ahead distribution market and integrate power losses and voltage constraints in DLMP. Since the first two levels are coupled, they are solved by reformulating it as a single level mathematical programming with equilibrium constraints (MPEC) by Karush-Kuhn-Tucker (KKT) optimality conditions and then mixed-integer linear programming (MILP) by the big-M method [26]. Once the optimal aggregated HVAC/EV schedule is obtained, the third level is solved to dispatch all participating residents based on the aggregated schedule. The main contributions are as follows:

1) The HVAC aggregator and EV aggregator models are developed on behalf of end users. In particular, a data generation and least-square parameter estimation (DG-LSPE) algorithm is applied to obtain the aggregated parameters of heterogeneous HVACs, which differs from the literature which assumes homogeneous HVACs.
2) A tri-level model is proposed for aggregators to manage the individual residents and to minimize the electricity payment as well as maintain the secure and economic operation of the distribution system. This is done in a competitive distribution market with DLMP as the electricity rate, which is different from many works assuming fixed rates or time-differentiated but pre-defined rates.
3) The analysis and results demonstrate and validate three main reasons, DLMP step changes, load shifts, and power loss reductions, which attribute to the payment saving for residential demands in a competitive DLMP market. Also, it is discovered that the step change pattern in DLMP can be caused by binding voltage constraints which have not been previously observed in the transmission-level LMP markets.

The rest of this paper is organized as follows. Section II describes the three-layer day-ahead distribution market structure and market participants including EV aggregator, HVAC aggregator, and DGs. Section III proposes the tri-level optimization model and presents the solution methods. Case studies in Section IV demonstrate the effectiveness of the proposed model and analyze both economic and operational benefits of flexible demand. Section V concludes the paper.

Fig. 1. Three-layer day-ahead distribution-level electricity market.

II. Structure and Participants of Distribution-Level Electricity Market

This section describes the structure of the distribution-level electricity market, roles and models of different participants.

A. Market Structure

In general, an individual resident is not eligible to participate in the market directly due to the complex market rules, strict participation requirements [27], and heavy calculation burden [20]. To address these challenges, aggregators have emerged to serve as intermediaries between these residents and DSO to provide demand flexibility. The structure of the three-layer distribution-level electricity market is illustrated in Fig. 1.

Based on Fig. 1, the roles of market participants are presented below.

1) DSO: The DSO is modeled as a balancing entity that is responsible for maintaining the safe and reliable operation of the distribution system. It is assumed that there are no other retailers in the distribution system, then the DSO can purchase electricity from the wholesale market and sell it to consumers. And the DSO provides a trading platform that enables transparent energy transactions between electricity producers and consumers, clears the market and broadcasts DLMP to the whole distribution system.

2) Aggregators: The aggregator has two tasks: i) collects comfortable temperature preferences and charging requirements of contracted residents, then calculates load quantities and submit them strategically to the DSO to reduce the energy payment, and ii) identifies the optimal allocation of the aggregated load to residential customers who may have HVAC and EV loads. Since the aggregator's bidding can influence DLMP, thus it is modeled as a price maker in this paper.

3) DGs: DGs like PV and MT are electricity producers, they participate in the market by providing a certain amount of electricity at a certain price to the DSO.

4) Fixed loads: They are modeled as the loads without price elasticity, forecasted according to the historical data, and considered as price takers.

5) HVAC and EV loads: HVAC and EV owners sign contracts with aggregators which help them respond to DLMP. And, the aggregator is assumed to have direct load control for individual buildings.

B. EV Aggregator

For the sake of simplicity, EV aggregators are assumed to locate at the same nodes with charging stations, and there are limited charging piles in each charging station. Thus, aggregated EV charging and discharging power are limited by this constraint. Here, the EV aggregator is modeled as the summation of all EVs.

$$E_{i,t+1} = E_{i,t} + \eta^C P^C_{i,t} - 1/\eta^D P^{Dri}_{i,t} \tag{1}$$

$$SOC_i^{E,\min} \cdot E_i^R \le E_{i,t+1} \le SOC_i^{E,\max} \cdot E_i^R \tag{2}$$

$$0 \le P^C_{i,t} \le P_i^{C,\max} \tag{3}$$

$$E_{i,t=0} \le E_{i,t=T} \tag{4}$$

$$\sum_{t=1}^{T} P^{Dri}_{i,t} = \sum_{j=1}^{N_i^e} e_j^d \cdot d_j \tag{5}$$

where (1) represents the energy of EV aggregator i, assuming all EVs have the same charging and discharging efficiency, (2) represents the state of charge (SOC) limits, (3) is the charging power limits, (4) ensures the total charging energy is no less than the total discharging energy over one day, (5) describes the driving consumption constraints, the sum of the energy consumption of individual EVs should be equal to that of aggregator model. $P_i^{C,max}$, E_i^R and $E_{i,t=0}$ are obtained as follows.

$$P_i^{C,\max} = \sum_{j=1}^{N_i^{piles}} p_j^C \tag{6}$$

$$E_i^R = \sum_{j}^{N_i^e} E_j^{rated} \tag{7}$$

$$E_{i,t=0} = \sum_{j}^{N_i^e} E_{j,t=0}. \tag{8}$$

C. HVAC Aggregator

1) Single HVAC: For simplicity, the first-order thermal transfer function is utilized to model a building's dynamic indoor temperature [12]. Thus, each HVAC in cooling mode can be modeled with the following equations:

$$\theta_{j,t+1} = a_j\theta_{j,t} + b_j\theta_{out,t} + g_j u_{j,t} \tag{9}$$

$$\theta^{\min} \le \theta_{j,t+1} \le \theta^{\max} \tag{10}$$

where $a_j = 1 - 1/C_jR_j$, $b_j = 1/C_jR_j$, $g_j = -\eta^H P^{rated} 1/C_j$.

2) HVAC Aggregator: Different from the analytical HVAC aggregation which assumes a homogeneous collection of HVACs [28], this paper supposes that HVACs are heterogeneous to ensure the diversity of individual buildings. Here, based on a typical house with parameters R_A and C_A, Gaussian distribution is applied to generate R_j and C_j to simulate physical differences among buildings. Then, a least squares-based approach, Algorithm 1, is proposed to estimate aggregated parameters. After that, the HVAC aggregator's thermal equation is modeled and corresponding operation constraints are presented below.

$$\tilde{\theta}_{i,t+1} = \tilde{a}_i\tilde{\theta}_{i,t} + \tilde{b}_i\theta_{out,t} + \tilde{g}_i\tilde{u}_{i,t} \tag{11}$$

Algorithm 1 DG-LSPE

Input HVACs' initial indoor temperatures $\theta_{j,t=0}$

Output Aggregated parameters $\tilde{a}, \tilde{b}, \tilde{g}$

Generate a data set: Simulate the dynamic indoor temperatures of N^h buildings in a whole day;
  Generate R_j and C_j for N^h buildings according to Gaussian distribution;
  for $\tilde{u}$ =0.1: 0.1: 1 **do**
    for t = 1: 1: T **do**
      Get the number of devices to be turned on: $N_{on} = N^h \cdot \tilde{u}$;
      Choose the top N_{on} HVACs to form the ON list ($u_{j,t}$ = 1) according to the descending order of $\theta_{j,t-1}$, and the rest form the OFF list ($u_{j,t}$ = 0);
      for j = 1, … N^h **do**
      Update $\theta_{j,t}$ by (9);
      end for
      Calculate average temperature $\tilde{\theta}_t$, and store [$\tilde{\theta}_t$, $\theta_{out,t}$, $\tilde{u}$] and $\tilde{\theta}_{t+1}$ separately;
    end for
  end for
Least squares parameter estimation:
  Obtain the aggregated parameters:

$$\boldsymbol{x} = \left(\boldsymbol{A}^T\boldsymbol{A}\right)^{-1}\boldsymbol{A}^T\boldsymbol{c}$$

$$P^H_{i,t} = \tilde{u}_{i,t} \cdot N_i^h \cdot P^{rated} \tag{12}$$

$$\theta^{\min} \le \tilde{\theta}_{i,t+1} \le \theta^{\max} \tag{13}$$

$$syn_i^{\min} \le \tilde{u}_{i,t} \le syn_i^{\max} \tag{14}$$

$$-\Delta\, u_i^{dr} \le \tilde{u}_{i,t+1} - \tilde{u}_{i,t} \le \Delta\, u_i^{ur} \tag{15}$$

$$SOC_i^{H,\min} \le SOC_{i,t} \le SOC_i^{H,\max} \tag{16}$$

where (11) represents the dynamic temperature of the HVAC aggregator, $\tilde{\theta}_{i,t} = \sum_{j=1}^{N_i^h}\theta_{j,t}\Big/N_i^h$, $\tilde{u}_{i,t} = \sum_{j=1}^{N_i^h}u_{j,t}\Big/N_i^h$, $\tilde{u}_{i,t}$ is approximated as a continuous variable in [0, 1], (12) is to obtain the active power of HVAC aggregator, (13) is comfortable temperature constraint, (14) is synchronicity constraint which limits the number of HVACs to be turned ON at the same period, (15) is ramp up/down constraint to limit the state transfer speed of HVACs, (16) is energy constraint to reduce the probability of all HVACs centering at the temperature boundaries [29] to improve the load dispatching performance. The $SOC_{i,t}$ is formulated as:

$$SOC_{i,t} = \frac{\sum_{j=1}^{N_i^h}\left(\theta_{\max} - \theta_{j,t}\right)}{N_i^h(\theta_{\max} - \theta_{\min})} = \frac{\theta_{\max} - \tilde{\theta}_{i,t}}{\theta_{\max} - \theta_{\min}}. \tag{17}$$

3) DG-LSPE: The HVAC control strategy plays an important role in the simulation of HVACs. Priority list control [30], a direct and effective control strategy, is utilized to control the state transformation of HVACs in this paper. Based on this, a DG-LSPE algorithm is designed to determine $\tilde{a}_i, \tilde{b}_i$ and $\tilde{g}_i$. Because every HVAC aggregator uses the same estimation algorithm, subscript i is neglected and procedures are described in Algorithm 1.

where

$$\begin{aligned}\boldsymbol{A}x &= \boldsymbol{c}, \boldsymbol{A} = [\boldsymbol{A}_{\tilde{u}=0.1}, \ldots, \boldsymbol{A}_{\tilde{u}=1}]^T,\\ \boldsymbol{c} &= [\boldsymbol{c}_{\tilde{u}=0.1}, \ldots, \boldsymbol{c}_{\tilde{u}=1}]^T,\\ \boldsymbol{A}_{\tilde{u}=k} &= \left[\left[\tilde{\theta}_1, \theta_{out,1}, \tilde{u}=k\right]; \ldots; \left[\tilde{\theta}_T, \theta_{out,T}, \tilde{u}=k\right]\right],\\ \boldsymbol{x} &= \left[\tilde{a}, \tilde{b}, \tilde{g}\right]^T, \boldsymbol{c}_{\tilde{u}=k} = \left[\tilde{\theta}_2, \ldots, \tilde{\theta}_{T+1}\right]^T.\end{aligned}$$

D. DG Models

According to the active or reactive power output and control strategy, most DGs fall into synchronous machines, inverter-based machines, and var compensation devices. For simplicity, three typical representatives are included in this paper.

MT is a synchronous machine-based DG. Its output power should satisfy the physical constraints and the power factor requirement [2]. In this paper, α_i is set to 0.95.

$$P_{i,t}^{MT,\min} \le P_{i,t}^{MT} \le P_{i,t}^{MT,\max} \tag{18}$$

$$0 \le Q_{i,t}^{MT} \le P_{i,t}^{MT} \tan(\arccos \alpha_i) \tag{19}$$

PV is an inverter-based generator that can both absorb or generate reactive power. The power factor range is [α_i lagging, α_i leading].

$$0 \le P_{i,t}^{PV} \le P_{i,t}^{PV,fore} \tag{20}$$

$$-P_{i,t}^{PV} \tan(\arccos \alpha_i) \le Q_{i,t}^{PV} \le P_{i,t}^{PV} \tan(\arccos \alpha_i) \tag{21}$$

Static Var compensator (SVC) is induced to help maintain the voltage due to three attributes: 1) can generate or absorb reactive power, 2) output power can be adjusted continuously, 3) a good tradeoff between cost and performance [2].

$$Q_{i,t}^{SVC,\min} \le Q_{i,t}^{SVC} \le Q_{i,t}^{SVC,\max}. \tag{22}$$

E. Uncertainty Consideration

The PV power output is of high uncertainty because it is easily influenced by the weather condition. To ensure the secure operation of the system, the power output is assumed to satisfy a certain confidence level η. Then the power output with chance constraints can be represented as:

$$P_r\left(P_{i,t}^{PV} \le P_{i,t}^{PV,fore}\right) \ge \eta \tag{23}$$

By equivalent transformations, (23) can be transformed as:

$$P_{i,t}^{PV} \le \bar{P}_{i,t}^{PV,fore} + \sigma_{i,t} \cdot \Phi_a^{-1}(1-\eta) \tag{24}$$

where Φ_a^{-1} is the inverse cumulative distribution function of standard normal distribution $N(0, 1^2)$, the forecasted PV power output $P_{i,t}^{PV,fore}$ is assumed to follow the Gaussian distribution, $P_{i,t}^{PV,fore} \sim N(\bar{P}_{i,t}^{PV,fore}, \sigma_{i,t}^2)$. Equation (20) is then modified by (24). The detailed derivation from (23) to (24) can be found in [31].

III. Tri-Level Model

As discussed in the previous section, aggregators and the DSO are different entities with different interests, meanwhile, an aggregator's load demand and the system DLMP are coupled variables, which means any change in one variable will cause changes in the other one and vice versa. Therefore, a bilevel model is formulated to represent this relationship. Next, since the aggregator and residents follow a vertical dispatcher-receiver structure, the third level model will allocate the demand to all participating residents after the aggregator's optimal load demand is determined.

A. First Level

The first level is to minimize aggregators' power purchasing costs while satisfying comforts and charging requirements.

$$\min \sum_{t\in T}\left(\sum_{i\in H} \pi_{i,t}^p \cdot P_{i,t}^H + \sum_{i\in E} \pi_{i,t}^p \cdot P_{i,t}^C\right) \tag{25a}$$

$$s.t.\ \text{constraints}(1)-(5), (11)-(17). \tag{25b}$$

B. Second Level

The second level is a market clearing model which has the objective to minimize system generation cost while maintaining all operational constraints. Note that the power congestion constraint is neglected in this study because congestion rarely happens in real distribution systems with radial topologies.

$$\min \sum_{t\in T}\left(\sigma_{S,t}^p \cdot P_{S,t}^G + \sigma_{S,t}^q \cdot \widehat{Q}_{S,t}^G + \sum_{i\in G}\left(\sigma_{i,t}^p \cdot P_{i,t}^G + \sigma_{i,t}^q \cdot \widehat{Q}_{i,t}^G\right)\right)$$
$$where\ G = \{PV, MT, SVC\} \tag{26a}$$

$$s.t.\ \sum_{i\in\{S,G\}} P_{i,t}^G - \sum_{i\in B} P_{i,t}^D - \sum_{i\in H} P_{i,t}^H - \sum_{i\in E} P_{i,t}^C - P_t^{loss} = 0 : \lambda_t^p, \forall t \in T \tag{26b}$$

$$\sum_{i\in\{S,G\}} Q_{i,t}^G - \sum_{i\in B} Q_{i,t}^D - Q_t^{loss} = 0 : \lambda_t^q, \forall t \in T \tag{26c}$$

$$V_{j,t} = V_{1,t} + \sum_{i\in B} Z_{j,i}^p\left(P_{i,t}^G - P_{i,t}^D - P_{i,t}^H - P_{i,t}^C\right) + \sum_{i\in B} Z_{j,i}^q\left(Q_{i,t}^G - Q_{i,t}^D\right) \tag{26d}$$

$$V^{\min} \le V_{j,t} \le V^{\max} : \omega_{j,t}^{v,\min}, \omega_{j,t}^{v,\max}, \forall j \in B, \forall t \in T \tag{26e}$$

$$P_{i,t}^{G,\min} \le P_{i,t}^G \le P_{i,t}^{G,\max} : \omega_{i,t}^{p,\min}, \omega_{i,t}^{p,\max}, \quad \forall i \in S, \forall t \in T \tag{26f}$$

$$Q_{i,t}^{G,\min} \le Q_{i,t}^G \le Q_{i,t}^{G,\max} : \omega_{i,t}^{q,\min}, \omega_{i,t}^{q,\max}, \quad \forall i \in S, \forall t \in T \tag{26g}$$

$$(18)(24) : \omega_{i,t}^{p,\min}, \omega_{i,t}^{p,\max}, \forall i \in \{MT, PV\}, \forall t \in T \tag{26h}$$

$$(19)(21)(22) : \omega_{i,t}^{q,\min}, \omega_{i,t}^{q,\max}, \forall i \in \{G\}, \forall t \in T \tag{26i}$$

$$-Q_{i,t}^G \le \widehat{Q}_{i,t}^G, Q_{i,t}^G \le \widehat{Q}_{i,t}^G : \kappa_{i,t}^-, \kappa_{i,t}^+, \forall i \in \{S, G\}, \forall t \in T \tag{26j}$$

where (26b) and (26c) represent the active and reactive power balance constraints, the substation is regarded as a generator with a large capacity; (26d) is the voltage expression derived from linearized power flow for distribution (LPF-D) [7], in which Z^p and Z^q are matrices of nodal voltage change with respect to net power injections that can be derived from [7];

(26e) is the voltage limit, Node 1 is the reference bus that connects to the substation; (26f) - (26i) are generators' active and reactive power output limits; in (26j), $\widehat{Q}^{G}_{i,t}= \left|Q^{G}_{i,t}\right|$ since both absorbing and generating reactive power will induce cost [2]. The power loss and power loss factors are obtained by the loss factors for distribution (LF-D) in [7], then the power loss is linearized by Taylor's series:

$$P^{loss}_{t} \approx P^{loss*}_{t} + \sum_{i\in B}\frac{\partial P^{loss}_{t}}{\partial P^{G}_{i,t}}\left(\Delta\ P^{G}_{i,t} - \Delta\ P^{D}_{i,t}\right) + \sum_{i\in B}\frac{\partial P^{loss}_{t}}{\partial Q^{G}_{i,t}}\left(\Delta\ Q^{G}_{i,t} - \Delta\ Q^{D}_{i,t}\right) \tag{27}$$

$$Q^{loss}_{t} \approx Q^{loss*}_{t} + \sum_{i\in B}\frac{\partial Q^{loss}_{t}}{\partial P^{G}_{i,t}}\left(\Delta\ P^{G}_{i,t} - \Delta\ P^{D}_{i,t}\right) + \sum_{i\in B}\frac{\partial Q^{loss}_{t}}{\partial Q^{G}_{i,t}}\left(\Delta\ Q^{G}_{i,t} - \Delta\ Q^{D}_{i,t}\right) \tag{28}$$

where $\Delta P^{G}_{i,t} = P^{G}_{i,t} - P^{G*}_{i,t}$ represents the power difference between two close operating points, $\Delta Q^{G}_{i,t}$, $\Delta P^{D}_{i,t}$ and $\Delta Q^{D}_{i,t}$ have similar expressions.

The decision variables are $P^{H}_{i,t}$ and $P^{C}_{i,t}$ in the first level objective function, $P^{G}_{S,t}$, $Q^{G}_{S,t}$, $P^{MT}_{i,t}$, $Q^{MT}_{i,t}$, $P^{PV}_{i,t}$, $Q^{PV}_{i,t}$, and $Q^{SVC}_{i,t}$ in the second level objective function.

The Lagrange function can be written as follows.

$$\begin{aligned} L = {} & \sum_{t\in T}\left(\sigma^{p}_{S,t}\cdot P^{G}_{S,t} + \sigma^{q}_{S,t}\cdot \widehat{Q}^{G}_{S,t} + \sum_{i\in G}\left(\sigma^{p}_{i,t}\cdot P^{G}_{i,t} + \sigma^{q}_{i,t}\cdot \widehat{Q}^{G}_{i,t}\right)\right) \\ & - \sum_{t\in T}\lambda^{p}_{t}\left(\sum_{i\in\{S,G\}} P^{G}_{i,t} - \sum_{i\in B} P^{D}_{i,t} - \sum_{i\in H} P^{H}_{i,t} - \sum_{i\in E} P^{C}_{i,t} - P^{loss}_{t}\right) \\ & - \sum_{t\in T}\lambda^{q}_{t}\left(\sum_{i\in\{S,G\}} Q^{G}_{i,t} - \sum_{i\in B} Q^{D}_{i,t} - Q^{loss}_{t}\right) \\ & - \sum_{t\in T}\sum_{j\in B}\omega^{v,\min}_{j,t}\left(V_{j,t} - V^{\min}\right) \\ & - \sum_{t\in T}\sum_{j\in B}\omega^{v,\max}_{j,t}\left(V^{\max} - V_{j,t}\right) \\ & - \sum_{t\in T}\sum_{i\in\{S,G\}}\omega_{i,t}\cdot g_{i,t}(x) \end{aligned} \tag{29}$$

where $g_{i,t}\ (x)$ represents the power output limits in (26f) - (26j).

The active DLMP is the first-order partial derivative of the Lagrange function with respect to the active power. According to (29), the active DLMP can be expressed as:

$$\pi^{p}_{i,t} = \frac{\partial L}{\partial P^{D}_{i,t}} = \lambda^{p}_{t} + \lambda^{p}_{t}\cdot\frac{\partial P^{loss}_{t}}{\partial P^{D}_{i,t}} + \lambda^{q}_{t}\cdot\frac{\partial Q^{loss}_{t}}{\partial P^{D}_{i,t}} + \sum_{j\in B}\left(\omega^{v,\min}_{j,t} - \omega^{v,\max}_{j,t}\right)Z^{p}_{j,i}. \tag{30}$$

Algorithm 2 HVAC Load Dispatching for Aggregator i

Input Optimal load $P^{H}_{i,t}$, HVACs' initial conditions and parameters $\theta_{j,t=0}$, R_j, C_j

Output ON/OFF status $u_{s,t}$, dispatching error $e_{i,t}$

```
for t = 1, ... T do
  for k = 1, ... K do
    s = (t-1)·K + k;
    Get the number of devices to be turned on:
    N_{k,on} = round(P^H_{i,t}/P^{rated});
    Update the ON/OFF status u_{j,s} based on N_{k,on} and
    the descending order of θ_{j,s-1};
    for j = 1, ... N^h_i do
      Update θ_{j,s} by (9);
      if θ_{j,s} > θ^{max}, then u_{j,s} = 1, N_{k,on} = N_{k,on} +1
      if θ_{j,s} < θ^{min}, then u_{j,s} = 0, N_{k,on} = N_{k,on} −1
    end for
  end for
  Calculate the accumulated dispatching error at t:
    e_{i,t} = ( P^H_{i,t} − Σ_{k=1}^{K} P^{rated}·N_{k,on}/K ) / P^H_{i,t} · 100%
end for
```

C. Third Level

The third level is to dispatch the optimal load demand for all individual end residents. Based on the priority list control, the load dispatching algorithm for HVACs, with a 10-min time step (i.e., K time slots in one hour, $K = 6$) to achieve more accurate control, is presented in Algorithm 2.

To make the EV charging close to practical situations, the individual EV is assumed to charge every few days with a longer charging time until reaching its upper SOC boundary. Based on this assumption, load dispatching for EV is similar to Algorithm 2, thus it is not shown here.

D. Solution Method of the Coupled First Two Levels

The first level and the second level are coupled due to the inter-dependent variables $P^{H}_{i,t}$, $P^{C}_{i,t}$ and $\pi^{p}_{i,t}$. The solution method for such a coupled bilevel model is described below.

1) MPEC Model: Since the second level is a linear programming problem, the KKT optimality conditions are the necessary and sufficient conditions of its optimal solution. Therefore, the bi-level optimization problem is transformed into a single level problem with the KKT conditions added to the first level. The new model is a single-level MPEC as:

$$\min\ (25a) \tag{31a}$$

$$s.t.\ \text{constraints } (25b), (26b) - (26d), (30) \tag{31b}$$

$$\sigma^{p}_{i,t} - \lambda^{p}_{t}\left(1 - \frac{\partial P^{loss}_{t}}{\partial P^{G}_{i,t}}\right) + \lambda^{q}_{t}\frac{\partial Q^{loss}_{t}}{\partial P^{G}_{i,t}} - \sum_{j\in B}\left(\omega^{v,\min}_{j,t} - \omega^{v,\max}_{j,t}\right)Z^{p}_{j,i} - \omega^{p,\min}_{i,t} + \omega^{p,\max}_{i,t} = 0, \forall i \in \{S, G\}, \forall t \in T \tag{31c}$$

$$\sigma^{q}_{i,t} - \kappa^{-}_{i,t} - \kappa^{+}_{i,t} = 0, \quad \forall i \in \{S, G\}, \forall t \in T \tag{31d}$$

$$\lambda^{p}_{t}\frac{\partial P^{loss}_{t}}{\partial Q^{G}_{i,t}} - \lambda^{q}_{t}\left(1 - \frac{\partial Q^{loss}_{t}}{\partial Q^{G}_{i,t}}\right) - \sum_{j\in B}\left(\omega^{v,\min}_{j,t} - \omega^{v,\max}_{j,t}\right)Z^{q}_{j,i} - \omega^{q,\min}_{i,t} + \omega^{q,\max}_{i,t} - \kappa^{-}_{i,t} + \kappa^{+}_{i,t} = 0,$$

$$\forall i \in \{S, G\}, \forall t \in T \tag{31e}$$

$$0 \le \omega_{j,t}^{v,\min} \perp \left(V_{j,t} - V^{\min}\right) \ge 0, \quad \forall j \in B, \forall t \in T \tag{31f}$$

$$0 \le \omega_{j,t}^{v,\max} \perp \left(V^{\max} - V_{j,t}\right) \ge 0, \quad \forall j \in B, \forall t \in T \tag{31g}$$

$$0 \le \omega_{i,t}^{p,\min} \perp \left(P_{i,t}^{G} - P_{i,t}^{G,\min}\right) \ge 0, \forall i \in \{S, G\}, \forall t \in T \tag{31h}$$

$$0 \le \omega_{i,t}^{p,\max} \perp \left(P_{i,t}^{G,\max} - P_{i,t}^{G}\right) \ge 0, \forall i \in \{S, G\}, \forall t \in T \tag{31i}$$

$$0 \le \omega_{i,t}^{q,\min} \perp \left(Q_{i,t}^{G} - Q_{i,t}^{G,\min}\right) \ge 0, \forall i \in \{S, G\}, \forall t \in T \tag{31j}$$

$$0 \le \omega_{i,t}^{q,\max} \perp \left(Q_{i,t}^{G,\max} - Q_{i,t}^{G}\right) \ge 0, \forall i \in \{S, G\}, \forall t \in T \tag{31k}$$

$$0 \le \kappa_{i,t}^{-} \perp \left(\widehat{Q}_{i,t}^{G} + Q_{i,t}^{G}\right) \ge 0, \forall i \in \{S, G\}, \forall t \in T \tag{31l}$$

$$0 \le \kappa_{i,t}^{+} \perp \left(\widehat{Q}_{i,t}^{G} - Q_{i,t}^{G}\right) \ge 0, \forall i \in \{S, G\}, \forall t \in T \tag{31m}$$

where (31c) - (31e) are stationary conditions, (31f) - (31m) are complementary slackness conditions which deal with the inequality constraints. The formulation of $0 \le \omega_{i,t} \perp h_{i,t}(x) \ge 0$ means both $\omega_{i,t}$ and $h_{i,t}(x)$ are no less than 0, and satisfy $\omega_{i,t} \cdot h_{i,t}(x) = 0$.

Noted that (31j) and (31k) including all DGs are written in the same generic expression for simplicity. They can be further elaborated based on constraints (19), (21) and (22) for specific DGs.

$$\begin{aligned}
&\sum_{t\in T}\left(\sum_{i\in H}\pi_{i,t}^{p}\cdot P_{i,t}^{H}+\sum_{i\in E}\pi_{i,t}^{p}\cdot P_{i,t}^{C}\right)\\
&=\sum_{t\in T}\sum_{i\in H}\left(\lambda_t^p+\lambda_t^p\frac{\partial P_t^{loss}}{\partial P_{i,t}^{D}}+\lambda_t^q\frac{\partial Q_t^{loss}}{\partial P_{i,t}^{D}}+\sum_{j\in B}(\omega_{j,t}^{v,\min}-\omega_{j,t}^{v,\max})Z_{j,i}^{p}\right)P_{i,t}^{H}\\
&\quad+\sum_{t\in T}\sum_{i\in E}\left(\lambda_t^p+\lambda_t^p\frac{\partial P_t^{loss}}{\partial P_{i,t}^{D}}+\lambda_t^q\frac{\partial Q_t^{loss}}{\partial P_{i,t}^{D}}+\sum_{j\in B}\left(\omega_{j,t}^{v,\min}-\omega_{j,t}^{v,\max}\right)Z_{j,i}^{p}\right)P_{i,t}^{C}\\
&=\sum_{t\in T}\left(\sigma_{S,t}^{p}\cdot P_{S,t}^{G}+\sigma_{S,t}^{q}\cdot\widehat{Q}_{S,t}^{G}+\sum_{i\in G}\left(\sigma_{i,t}^{p}\cdot P_{i,t}^{G}+\sigma_{i,t}^{q}\cdot\widehat{Q}_{i,t}^{G}\right)\right)\\
&\quad-\left\{\begin{array}{l}
\sum_{t\in T}\lambda_t^p\left(\sum_{i\in B}\left(1+\frac{\partial P_t^{loss}}{\partial P_{i,t}^{D}}\right)P_{i,t}^{D}+\sum_{i\in B}\frac{\partial P_t^{loss}}{\partial Q_{i,t}^{D}}Q_{i,t}^{D}+P_t^{loss0}\right)\\
+\sum_{t\in T}\lambda_t^q\left(\sum_{i\in B}\left(1+\frac{\partial Q_t^{loss}}{\partial Q_{i,t}^{D}}\right)Q_{i,t}^{D}+\sum_{i\in B}\frac{\partial Q_t^{loss}}{\partial P_{i,t}^{D}}P_{i,t}^{D}+Q_t^{loss0}\right)\\
+\sum_{t\in T}\sum_{j\in B}\omega_{j,t}^{v,\min}\left(V^{\min}-V_{1,t}+\sum_{i\in B}Z_{j,i}^{p}P_{i,t}^{D}+\sum_{i\in B}Z_{j,i}^{q}Q_{i,t}^{D}\right)\\
-\sum_{t\in T}\sum_{j\in B}\omega_{j,t}^{v,\max}\left(V^{\max}-V_{1,t}+\sum_{i\in B}Z_{j,i}^{p}P_{i,t}^{D}+\sum_{i\in B}Z_{j,i}^{q}Q_{i,t}^{D}\right)\\
+\sum_{t\in T}\sum_{i\in\{S,G\}}\left(\omega_{i,t}^{p,\min}P_{i,t}^{G,\min}-\omega_{i,t}^{p,\max}P_{i,t}^{G,\max}\right)\\
+\sum_{t\in T}\sum_{i\in\{S,G\}}\left(\omega_{i,t}^{q,\min}Q_{i,t}^{G,\min}-\omega_{i,t}^{q,\max}Q_{i,t}^{G,\max}\right)
\end{array}\right\}.
\end{aligned}\tag{32}$$

2) MILP Model: From the above formulation, it can be seen that MPEC is a nonlinear model with nonlinearities in two parts: 1) $\pi_{i,t}^{p} \cdot P_{i,t}^{H} + \pi_{i,t}^{p} \cdot P_{i,t}^{C}$ in the objective function (31a); 2) complementary slackness constraints (31f) - (31m). The methods for dealing with these nonlinearities are described below [32], [33].

For $\pi_{i,t}^{p} \cdot P_{i,t}^{H} + \pi_{i,t}^{p} \cdot P_{i,t}^{C}$, the strong duality theory states that the primal problem and its dual problem have the same optimal value if the problem is convex. The original second level is a linear optimization model, thus (31a) can be substituted by (32).

For the complementary constraints, the big-M approach is adopted. Then, each formulation of $0 \le \omega_{i,t} \perp h_{i,t}(x) \ge 0$ can be substituted as:

$$0 \le \omega_{i,t} \le M_{i,t} v_{i,t}, 0 \le h_{i,t}(x) \le M_{i,t}\left(1 - v_{i,t}\right) \tag{33}$$

where $M_{i,t}$ is a big number and $v_{i,t}$ is a binary variable.

Now, the completed MILP model is presented as:

$$min \ \ (32) \tag{34a}$$

$$s.t. \ \ \text{constraints}(31b) - (31e), (33) \tag{34b}$$

After the MILP model is solved, Algorithm 2 is applied to dispatch the aggregated load to all end residents, as discussed in the previous Section III-C.

It should be noted that the proposed tri-level approach is based on a competitive DLMP model, which is aligned with the increasing interests in industrial practices toward competitive distribution or retail markets [34].

TABLE I
PARAMETERS OF SINGLE EV AND HVAC

EV	Parameter	HVAC	Parameter
E_j^{rated}	N (50, 1^2) (kWh)	P^{rated}	5 (kW)
P_j^{C}	N (7.2, 0.2^2) (kW)	R_j	N (R_A, 0.2^2) (°C/kW)
e_j^{d}	N (0.23, 0.01^2) (kWh/mile)	C_j	N (C_A, 0.2^2) (kWh/°C)
η^C/η^D	0.98	η^H	3
$E_{j,t=0}$	$E_j^{rated} \cdot U$ [0.4,0.6] (kWh)	θ^{max}	21 (°C)
d_j	U [30, 50] (miles)	θ^{min}	19 (°C)

IV. CASE STUDIES

In this section, the proposed tri-level model is tested on a modified IEEE 33-Bus distribution system. Simulations are performed on a laptop with Intel Core i7-8650U 2.11GHz CPU, and 16GB RAM. The coding work is carried out in MATLAB R2019a, YALMIP and CPLEX 12.9.

A. IEEE 33-Bus Distribution System

The topology of the modified IEEE 33-Bus system is shown in Fig. 2, in which two 500 kW PVs are installed at nodes 12 and 28, respectively; two 500 kW MTs are located at nodes 18 and 33, respectively; and three 500 kVar SVCs are installed at nodes 10, 16 and 30, respectively. The parameters of a single EV and HVAC, EV aggregators and HVAC aggregators are shown in Table I and Table II respectively. Here, it is assumed that HVAC units in their corresponding aggregator have similar thermal parameters, and have a big difference with HVAC units in other aggregators.

The day-ahead active LMP of the wholesale market, scaled forecasted mean power output of PV and scaled fixed load are obtained from PJM [35], as depicted in Fig. 3 (a). It is assumed the standard deviation of the forecasted PV is 15% of the mean value and the confidence level η is 0.95. The system peak fixed load is 3.715MW + j1.78MVar. The active power bidding prices of PV and MT are set to \$15/MWh and \$70/MWh, respectively. Reactive LMP, reactive power prices

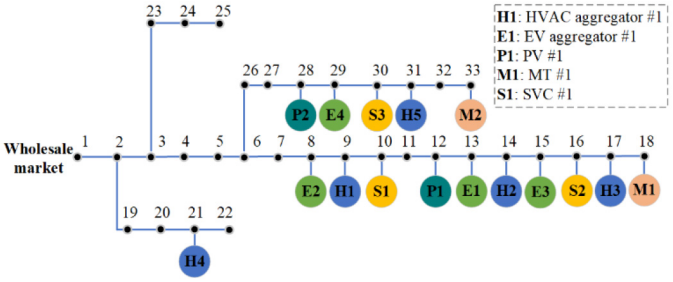

Fig. 2. Modified IEEE 33-Bus system.

TABLE II
PARAMETERS OF AGGREGATORS

Aggregators	Parameter	Typical Value
HVAC Aggregators	Location	Node 9, 11, 17, 21, 31
	Number of HVACs	160, 160, 320, 320, 320
	R_A (°C/kW)	3.96, 3.6, 3.96, 4.32, 4.68
	C_A (kWh/°C)	3.75
	Synchronization limit	[0.1, 0.7]
	SOC limit	[0.15, 0.8]
	Ramp up/down rate	0.1
EV Aggregators	Location	Node 8, 13, 15, 29
	Number of EVs	300, 300, 300, 300
	Number of chargers	25, 25, 25, 25
	SOC limit	[0.2, 0.8]

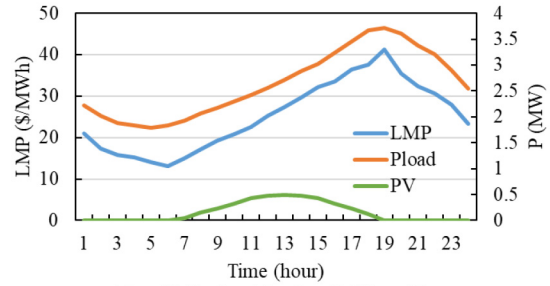

(a) LMP, fixed load and PV profiles

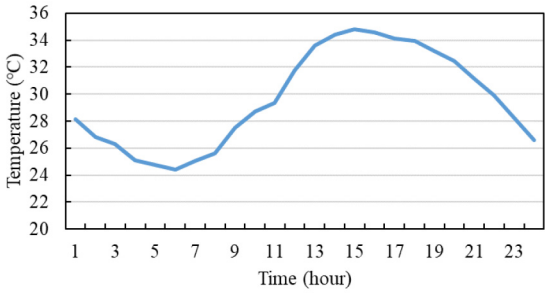

(b) Outdoor temperature

Fig. 3. LMP, fixed load, PV, and outdoor temperature on a summer day.

of PV, MT and SVC are set to 0. The outdoor temperature on a summer day is shown in Fig. 3 (b).

Aggregators can choose to participate in the market or not. If they participate in the market, their loads become flexible; otherwise, they are only price takers and are regarded as fixed loads. Five cases with different flexible load ratios are established in Table III. The flexible load ratio is defined as the maximum ratio of flexible load divided by the system load.

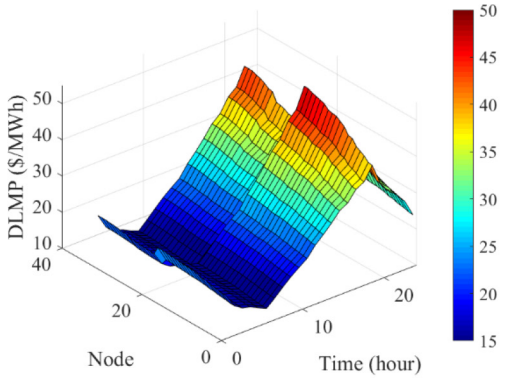

(a) DLMP

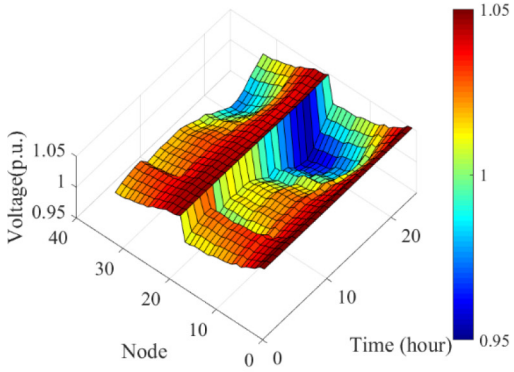

(b) Voltage

Fig. 4. Spatial and temporal distribution of DLMPs and voltages.

TABLE III
DIFFERENT CASES

Case	Flexible ratio	Load composition		
		Flexible load	**Total fixed loads**	
0	0%	None	H1 - H5, E1 - E4	Other fixed loads
1	10%	H1 - H2, E1	H3 - H5, E2 - E4	Other fixed loads
2	20%	H1 - H3, E1 - E2	H4 -H5, E3 - E4	Other fixed loads
3	30%	H1 - H4, E1 - E3	H5, E4	Other fixed loads
4	40%	H1 - H5, E1 - E4	None	Other fixed loads

B. Analysis of Case 1

1) DLMP and Voltage Profiles: The DLMP and voltage profiles of all nodes for 24 hours are shown in Fig. 4. It can be seen in Fig. 4 (a) that DLMP increases as the node number increases. This is due to the radial topology and power loss is a component of DLMP. The farther away from Node 1, the larger the power loss factor will be. Fig. 4 (b) shows that voltages are maintained within the voltage boundary.

2) HVAC Aggregator: H2's load demand and its corresponding buildings' indoor temperatures are shown in Fig. 5. From Fig. 5 (a), it can be seen that load shift happens. Combined with Fig. 4 (a), it is revealed that incentivized by DLMP, an aggregator consumes more energy before price arises. According to the indoor temperatures in Fig. 5 (b), this load shifting is the precooling for HVACs.

3) EV Aggregator: E1's load profile under Case 0 and Case 1 are shown in Fig. 6 (a). In Case 0, it is assumed EV owners choose to charge during daytime and charging power

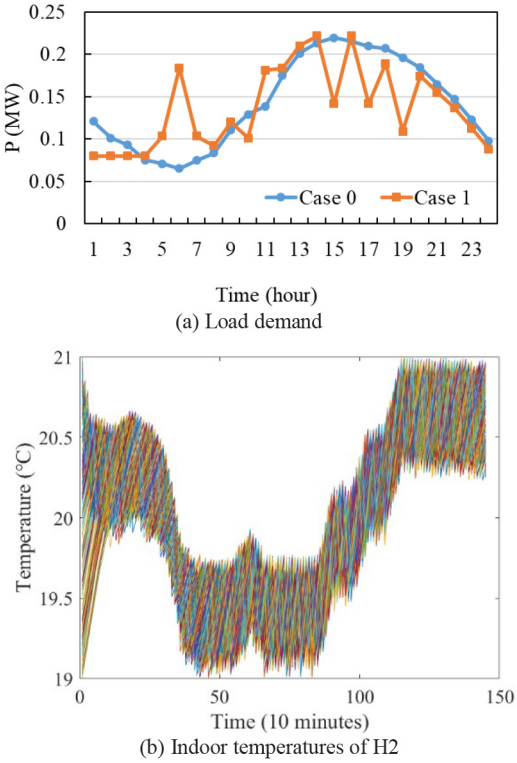

(a) Load demand

(b) Indoor temperatures of H2

Fig. 5. H2's load demand and indoor temperatures.

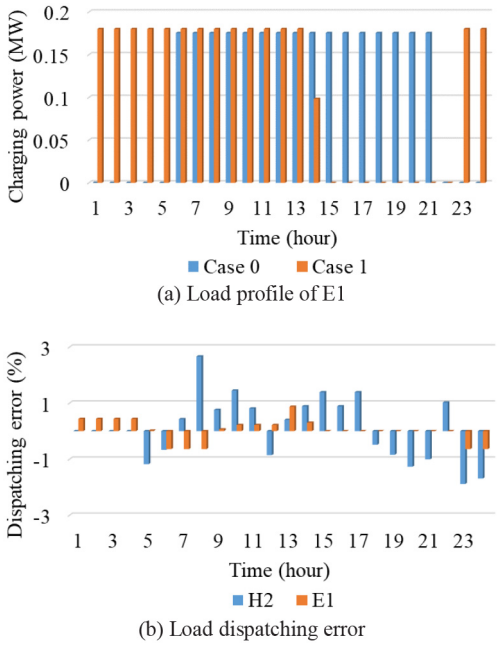

(a) Load profile of E1

(b) Load dispatching error

Fig. 6. Load profile of E1 and load dispatching error of H2 and E1.

is evenly distributed at different hours to simplify the charging process. While in Case 1, the EV aggregator makes the optimal charging schedule, such that the charging process happens during 1:00 - 14:00 and 23:00 - 24:00 when DLMP is not high.

4) Load Dispatching Error Analysis: The load dispatching errors of H2 and E1 in Case 1 are shown in Fig. 6 (b). The accumulated dispatching errors (i.e., $e_{i,t}$ in Step 12, Algorithm 2) are within $\pm 3\%$ at each hour, which indicates the effectiveness of the proposed aggregator model and the power dispatch algorithm.

TABLE IV
ABSOLUTE MAXIMUM DISPATCH ERROR UNDER DIFFERENT GAUSSIAN PARAMETERS

σ (Sk=0)	0	0.1	0.2	0.3	0.4	0.5	0.6
max $\lvert e_{i,t}\rvert$	2.438	2.064	2.663	1.996	2.573	3.778	7.109
Sk (σ=0.2)	-0.6	-0.4	-0.2	0	0.2	0.4	0.6
max $\lvert e_{i,t}\rvert$	1.671	2.174	2.595	2.663	3.34	2.283	3.625

where max $|e_{i,t}|$ refers to the maximum absolute dispatch error.

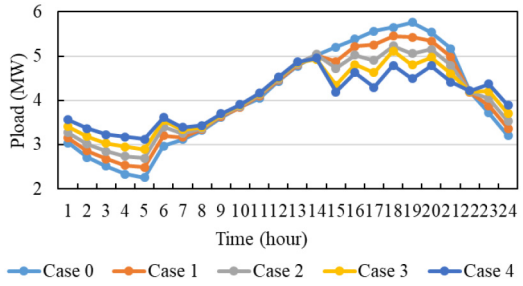

Fig. 7. System load profiles under different flexible ratios.

In Table I, parameters of individual HVACs and EVs are assumed to follow the Gaussian distribution. To provide an in-depth analysis of the impacts of Gaussian distribution on the dispatching error, additional simulations are shown next. For simplicity, we may have HVAC as the research target, and assume that R_j and C_j satisfy the following Gaussian parameters: 1) no skewness ($Sk = 0$), different standard deviation (σ); 2) fixed standard deviation ($\sigma = 0.2$), different skewness. The simulation results are shown in Table IV.

From Table IV, it can be observed that: 1) with the increase of standard deviation, the absolute maximum dispatch error in the 24-hour time scale is in an increasing trend. This indicates that a higher difference level will result in a higher maximum absolute dispatch error, however, it is under 8% which is acceptable; 2) when fixing the standard deviation and varying the skewness of the Gaussian distribution, the scale of the maximum absolute dispatch error keeps at the same level, this shows that the skewness does not impact the dispatch error. This is reasonable because Algorithm 1 is a generic method that can deal with the skewness distribution and can reflect the skewness into the aggregated parameters and then Algorithm 2 can well dispatch the load.

It should be noted that the different max $|e_{i,t}|$ in each simulation is due to the random sampling of R_j and C_j according to the different Gaussian distribution parameters.

C. Operation and Economic Analysis Under Different Flexible Load Ratios

System load profiles under different flexible ratios in 24 hours are shown in Fig. 7, and voltage profiles at t = 19:00 are shown in Fig. 8. From Fig. 7 and Fig. 8, it can be observed that with the increase of flexible load ratio, peak load is further reduced, more load is shifted from peak hours to off-peak hours, and the voltage profiles at peak hours are improved.

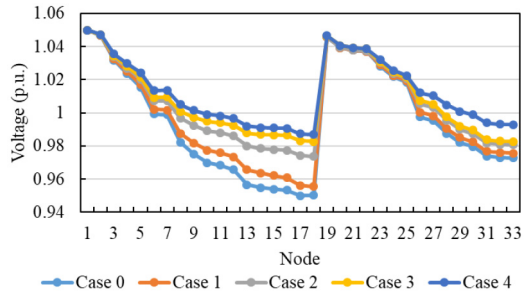

Fig. 8. Voltage profiles of at t = 19:00 under different flexible ratios.

TABLE V
BENEFITS OF DLMP TO THE SYSTEM WITH UNCERTAINTY

Case	Operation		Economy				
	P^* (MW)	V^* (p.u.)	GC ($)	HVAC and EV Payment ($)			
				Total	Enr.	Vol.	Loss
0	5.76	0.95	2712.4	1163.7	964.8	40.2	158.7
1	5.43	0.954	2660.3	1043.8	931.5	0	112.2
2	5.06	0.973	2609.5	976.5	900.9	0	75.6
3	4.80	0.983	2568.3	932.3	870.7	0	61.7
4	4.49	0.987	2526.2	886.3	840.2	0	46.1

TABLE VI
BENEFITS OF DLMP TO THE SYSTEM WITHOUT UNCERTAINTY

Case	Operation		Economy				
	P^* (MW)	V^* (p.u.)	GC ($)	HVAC and EV Payment ($)			
				Total	Enr.	Vol.	Loss
0	5.76	0.950	2682.0	1158.3	964.8	40.4	153.2
1	5.39	0.957	2630.8	1039.1	931.7	0	107.5
2	5.02	0.975	2580.4	972.4	901.0	0	71.4
3	4.78	0.984	2538.4	928.6	870.8	0	57.8
4	4.47	0.988	2497.7	882.9	840.3	0	42.5

Part of the numerical results are shown in Table V, in which P^* refers to the system load at t = 19:00; V^* refers to the voltage at node 18 at t = 19:00; GC is the total system generation cost; Enr., Vol., and Loss are energy cost, voltage support cost and power loss cost of HVAC and EV payment, respectively. When compare Case 4 with Case 0, it can be seen that peak load, total generation cost, total HVAC and EV electricity payment are reduced by 22.05%, 6.87% and 23.84%, and voltage is improved by 3.90%, respectively. Due to load shift, the DSO reduces the cost of purchasing electricity from the wholesale market and the cost of scheduling peaking DG units (MT in this paper) at high LMP hours. The analysis of HVAC and EV payment reduction is presented in detail in Section IV-D.

The simulation results without PV uncertainty are shown in Table VI. Compared with Table V, it can be found that both the operational benefits and the economic benefits of Table V are less than that of Table VI, which means the introduction of uncertainty leads to more conservative results.

Regarding the computational aspects, in Case 4 with all HVACs and EVs are considered, the MILP formulation has 6698 constraints, 5697 continuous variables, and 2736 binary variables in total. The average calculation time of 10 simulation runs is 24.246s, where Algorithm 1 takes 0.035s, MILP takes 24.189s, and Algorithm 2 takes 0.022s. Since the MILP is a large-scale optimization problem, it takes much more calculational time than that of Algorithm 1 and Algorithm 2.

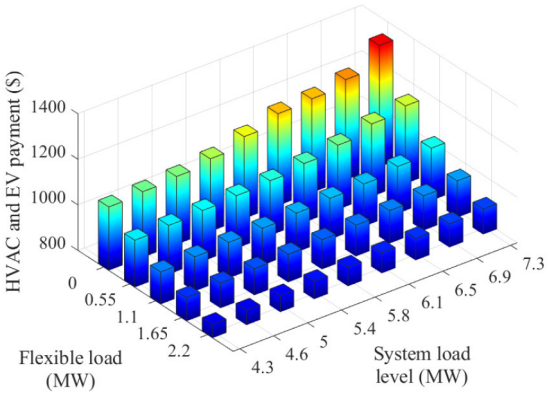

(a) HVAC and EV payment in the 3-dimension view

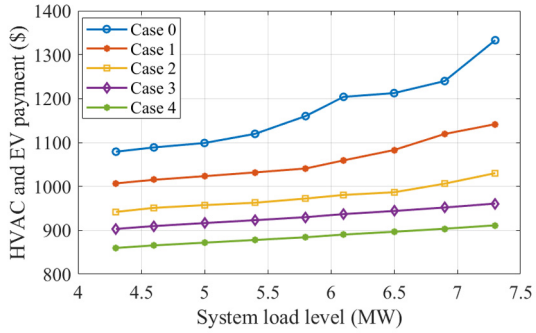

(b) HVAC and EV payment in the 2-dimension view

Fig. 9. HVAC and EV payment versus different load levels with various flexible loads.

D. Economic Analysis Under Different System Load Levels

In this subsection, simulations are carried out to investigate the impacts of the system load level. The fixed load is varied from 0.6 to 1.4 times the original fixed load shown in Fig. 3 (a). The numbers of HVACs and EVs are kept the same as in Table II. The system load level is defined as the peak load in Case 0. As illustrated in Fig. 9, the system load level ranges from 4.3 MW to 7.3 MW, the flexible load of the five cases is between 0 and 2.2 MW.

From Fig. 9, we have three findings regarding the economic benefits from demand flexibility:

1) **F1:** At the same system load level, a higher flexible load can significantly reduce the payment which has the same pattern as in Table V.
2) **F2:** With the same flexible load, HVACs and EVs payment increases as the system total load increases (i.e., fixed load increases).
3) **F3:** In addition to **F2**, the increased payments between 4.3 and 7.3 MW system load levels are different for five cases. The increasing rates are 23.54%, 13.39%, 9.31%, 6.39%and 6.00%, respectively, which indicates a higher flexible load can slow down the payment increase rate. This is shown by the payment curves of the five cases in Fig. 9 (b). The detailed increment can be found in Table VII.

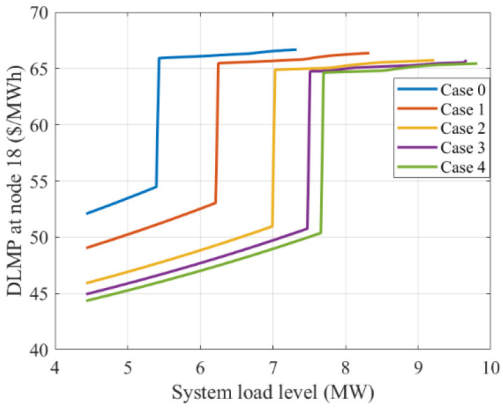

Fig. 10. DLMP at node 18 with step changes under different system load levels.

TABLE VII
PAYMENT INCREASE AND ITS DECOMPOSITION BETWEEN 4.3 AND 7.3 MW SYSTEM LOAD LEVEL

Case	ΔPayment ($)	Inc. ratio (%)	Decomposition ($)		
			ΔEnr.	ΔVol.	ΔLoss
0	253.99	23.54%	0	167.06	86.93
1	134.85	13.39%	0.39	62.58	71.89
2	87.92	9.31%	3.15	24.89	59.88
3	57.72	6.39%	2.4	0	54.69
4	51.55	6.00%	1.78	0	48.70

As equation (30) shows, DLMP consists of three parts: energy price, voltage support price and power loss price. Accordingly, HVAC and EV electricity payments can also be decomposed into three components as shown in Table V and Table VII. Based on observations from these two tables, the fundamental reasons of the three findings can be summarized as follows.

1) **Load shifts:** In general, if shifting loads from peak DLMP hours to off-peak DLMP hours, the energy cost can be reduced. Table V and the discussion in Section IV-C demonstrate that with more flexible loads, the load-shifting quantity increases and energy cost decreases. This is an important reason of the finding **F1**. Also, with the same flexible load and an increasing total system load, the load-shifting quantity keeps almost the same. As can be found in Table VII, Δ Enr. is close to 0 for five cases, thus energy cost contributes little to the findings **F2** and **F3**.
2) **DLMP step changes:** To illustrate this, Fig. 10 shows the DLMP at node 18 at $t = 19{:}00$ under different system load levels. The simulation for each case ends at its own operation capacity. It can be seen that DLMP spikes up at a certain load level. In this study, the step change of DLMP is similar to that of LMP in [36]. However, the difference is that the former is caused by the binding voltage limit while the latter is the binding congestion limit. Taking Case 0 as an example, when the system load is beyond 5.3 MW, DLMP has a sudden increase because the voltage limit at node 18 binds, and M1 is activated to support the voltage at node 18. The comparison in Table V and Table VII clearly shows that at the same system load level, the more flexible loads, the less likely having binding voltage limits, thus less voltage support cost. More importantly, when the system load increases from 4.3 to 7.3 MW, Cases 0, 1 & 2 have a sharper increase than Cases 3 & 4 because DLMP step changes of Cases 0-2 come quicker as shown in Fig. 10. This DLMP step change is a hidden reason related to all the findings **F1**∼**F3**.
3) **Power losses:** As shown in Fig. 10, before reaching the step change, DLMP has a slight but consistent increase which is because of power losses. Equation (30) shows that the power loss price is proportional to power loss factors, which are generally higher in peak hours than that in off-peak hours. Therefore, the loss prices in peak hours are higher than in off-peak hours, and the power loss cost can be reduced by load shifting as well. All three findings **F1**∼**F3** are related to power losses.

The above three reasons can serve as general guidelines for decision-makers to carefully choose the appropriate time and location of HVACs and EVs to potentially gain high benefits.

V. CONCLUSION

In this paper, DLMP is used as price signals to guide the electricity consumption of residential customers. In the day-ahead distribution market environment, a tri-level scheduling model is proposed to minimize residents' electricity bills. Two algorithms are designed to aggregate and dispatch individual customers. KKT optimality conditions, big-M method and strong duality theory are utilized to solve the coupled first two levels. Numerical studies show the following conclusions:

1) The proposed DG-LSPE algorithm can estimate the aggregated HVAC parameters under different Gaussian distribution parameters, and the collaboration with the subsequent load dispatching algorithm can control the dispatching error to a limited range.
2) The tri-level scheduling model quantitively demonstrates the potentials of operational and economic benefits for both the distribution system and aggregators, especially in different flexible load ratios.
3) By the in-depth analysis of DLMP components and payment components, three generalized reasons leading to the benefit from flexible HVAC and EV demands are summarized, namely, load shifts, DLMP step changes, and power losses. This can be used by stakeholders for better decision-making.

APPENDIX
ADDITIONAL DISCUSSION ON DLMP STEP CHANGE

In Fig. 10, the DLMP does not go to \$70/MWh which is the active power bidding price of MT. The main reason is: in the distribution system, voltage constraint involves both active power and reactive power even if in a linearized model, such as (26d). This means reactive power can also contribute to the voltage profile. In the MT model (18),(19), MT generates both active power and reactive power. Therefore, once the MT is turned on, both active power and reactive power will support the voltage. Meanwhile, in Section IV, the reactive power price

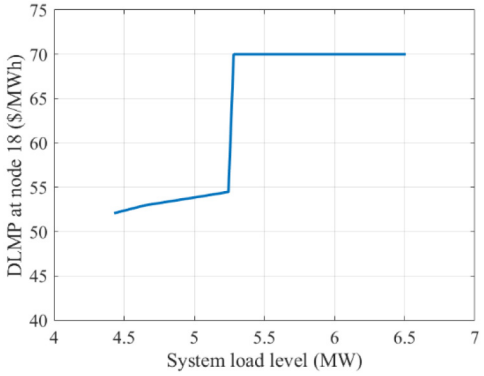

Fig. A1. DLMP with step changes under different system load levels.

is set to 0. Thus, regarding voltage improvement by the same amount, the active power provided by MT is less than that of the MW-only provider. Therefore, under the same active power price, the marginal voltage support cost of the former should be less than that of the latter.

To make this point clearer, here is an example. The task is to improve the voltage at node 18 by ΔV.

1) Scenario 1: MT provides active power $\Delta P1>0$ and reactive power $\Delta Q1>0$. The additional cost is $\$70\cdot\Delta P1+\$0\cdot\Delta Q1 = \$70\cdot\Delta P1$.
2) Scenario 2: MT provides active power $\Delta P2>0$ and reactive power $\Delta Q2 = 0$. The additional cost is $\$70\cdot\Delta P2$.

Then we could have $\Delta P1 < \Delta P2$ because there is no reactive power support in Scenario 2 which demands more real power to raise the voltage. Since $\Delta P1 < \Delta P2$, we have $\$70\cdot\Delta P1 < \$70\cdot\Delta P2$. If $\Delta P2 = 1$, it means the marginal cost (DLMP) of Scenario 2 is \$70/MWh, and DLMP of Scenario 1 is less than \$70/MWh. This is the reason why the DLMP at node 18 does not reach \$70/MWh.

Finally, based on Scenario 2, a new simulation is carried out: assume MT only provides active power and does not provide reactive power. Based on Case 0, the DLMP under different system load levels is shown in Fig. A1. It can be observed that the DLMP at node 18 reaches \$70/MWh, which validates the above reasoning. Similar patterns can also be found from Case 1 to Case 4 which are not elaborated here.

DISCLAIMER

REFERENCES

[1] K. Horowitz *et al.*, "An overview of distributed energy resource (DER) interconnection: Current practices and emerging solutions," NREL, Denver, CO, USA, Rep. NREL/TP-6A20-72102, Apr. 2019.

[2] L. Bai, J. Wang, C. Wang, C. Chen, and F. Li, "Distribution locational marginal pricing (DLMP) for congestion management and voltage support," *IEEE Trans. Power Syst.*, vol. 33, no. 4, pp. 4061–4073, Jul. 2018.

[3] R. R. Mohassel, A. Fung, F. Mohammadi, K. Raahemifar, "A survey on advanced metering infrastructure," *Int. J. Elect. Power Energy Syst.*, vol. 63, pp. 473–484, Dec. 2014.

[4] P. O. Rosell *et al.*, "Optimization problem for meeting distribution system operator requests in local flexibility markets with distributed energy resources," *Appl. Energy*, vol. 210, pp. 881–895, Jan. 2018.

[5] F. Li and R. Bo, "DCOPF-based LMP simulation: Algorithm, comparison with ACOPF, and sensitivity," *IEEE Trans. Power Syst.*, vol. 22, no. 4, pp. 1475–1485, Nov. 2007.

[6] P. M. Sotkiewicz and J. M. Vignolo, "Nodal pricing for distribution networks: Efficient pricing for efficiency enhancing DG," *IEEE Trans. Power Syst.*, vol. 21, no. 2, pp. 1013–1014, May 2006.

[7] H. Yuan, F. Li, Y. Wei, and J. Zhu, "Novel linearized power flow and linearized OPF models for active distribution networks with application in distribution LMP," *IEEE Trans. Smart Grid*, vol. 9, no. 1, pp. 438–448, Jan. 2018.

[8] Y. K. Renani, M. Ehsan, and M. Shahidehpour, "Optimal transactive market operations with distribution system operators," *IEEE Trans. Smart Grid*, vol. 9, no. 6, pp. 6692–6701, Nov. 2018.

[9] Q. Hou, N. Zhang, J. Yang, C. Kang, Q. Xia, and M. Miao, "Linearized model for active and reactive LMP considering bus voltage constraints," in *Proc. IEEE Power Energy Soc. Gen. Meeting*, Portland, OR, USA, 2018, pp. 1–5.

[10] W. Wei, Z. Shen, L. Wu, F. Li, and T. Ding, "Estimating DLMP confidence intervals in distribution networks with AC power flow model and uncertain renewable generation," *IET Gener. Transm. Distrib.*, vol. 14, no. 8, pp. 1467–1475, Apr. 2020.

[11] R. Mowris and E. Jones, "Peak demand and energy savings from properly sized and matched air conditioners," in *Proc. ACEEE Summer Study Energy Efficiency Build.*, Pacific Grove, CA, USA, 2008, pp. 196–208.

[12] Q. Shi, C.-F. Chen, A. Mammoli, and F. Li, "Estimating the profile of incentive-based demand response (IBDR) by integrating technical models and social-behavioral factors," *IEEE Trans. Smart Grid*, vol. 11, no. 1, pp. 171–183, Jan. 2020.

[13] A. Roth and J. Reyna, "Grid-interactive efficient buildings technical report series: Whole-building controls, sensors, modeling, and analytics," NREL, Denver, CO, USA, Rep. NREL/TP-5500-75478 and DOE/GO-102019-5230, Dec. 2019.

[14] H. Zhong, L. Xie, and Q. Xia, "Coupon incentive-based demand response: Theory and case study," *IEEE Trans. Power Syst.*, vol. 28, no. 2, pp. 1266–1276, May 2013.

[15] A. D. Giorgio and L. Pimpinella, "An event driven smart home controller enabling consumer economic saving and automated demand side management," *Appl. Energy*, vol. 96, pp. 92–103, Aug. 2012.

[16] K. Herter and S. Wayland, "Residential response to critical-peak pricing of electricity: California evidence," *Energy*, vol. 35, pp. 1561–1567, Apr. 2010.

[17] J. Vuelvas and F. Ruiz, "Rational consumer decisions in a peak time rebate program," *Elect. Power Syst. Res.*, vol. 143, pp. 533–543, Feb. 2017.

[18] S. Bhattacharya, K. Kar, and J. H. Chow, "Optimal precooling of thermostatic loads under time-varying electricity prices," in *Proc. IEEE Amer. Control Conf. (ACC)*, Seattle, WA, USA, 2017, pp. 1407–1412.

[19] Y.-J. Kim, "Optimal price based demand response of HVAC systems in multizone office buildings considering thermal preferences of individual occupants buildings," *IEEE Trans. Ind. Informat.*, vol. 14, no. 11, pp. 5060–5073, Nov. 2018.

[20] X. Kou *et al.*, "A scalable and distributed algorithm for managing residential demand response programs using alternating direction method of multipliers (ADMM)," *IEEE Trans. Smart Grid*, vol. 11, no. 6, pp. 4871–4882, Nov. 2020.

[21] M. Ostadijafari, R. R. Jha, and A. Dubey, "Demand-side participation via economic bidding of responsive loads and local energy resources," *IEEE Open Access J. Power Energy*, vol. 8, pp. 11–22, 2021.

[22] R. Li, Q. Wu, and S. S. Oren, "Distribution locational marginal pricing for optimal electric vehicle charging management," *IEEE Trans. Power Syst.*, vol. 29, no. 1, pp. 203–211, Jan. 2014.

[23] S. Huang, Q. Wu, S. S. Oren, R. Li, and Z. Liu, "Distribution locational marginal pricing through quadratic programming for congestion management in distribution networks," *IEEE Trans. Power Syst.*, vol. 30, no. 4, pp. 2170–2178, Jul. 2015.

[24] W. Liu, Q. Wu, F. Wen, and J. Østergaard, "Day-ahead congestion management in distribution systems through household demand response and distribution congestion prices," *IEEE Trans. Smart Grid*, vol. 5, no. 6, pp. 2739–2747, Nov. 2014.

[25] P. Siano and D. Sarno, "Assessing the benefits of residential demand response in a real time distribution energy market," *Appl. Energy*, vol. 161, pp. 533–551, Jan. 2016.
[26] J. Fortuny-Amat and B. McCarl, "A representation and economic interpretation of a two-level programming problem," *J. Oper. Res. Soc.*, vol. 32, no. 9, pp. 783–792, Sep. 1981.
[27] D. S. Kirschen and G. Strbac, *Fundamentals of Power System Economics*, 2nd ed. Jersey City, NJ, USA: Wiley, 2018.
[28] B. M. Sanandaji, T. L. Vincent, and K. Poolla, "Ramping rate flexibility of residential HVAC loads," *IEEE Trans. Sustain. Energy*, vol. 7, no. 2, pp. 865–874, Apr. 2016.
[29] J. Dong *et al.*, "Battery equivalent model for residential HVAC," in *Proc. IEEE Power Energy Soc. Gen. Meeting*, Montreal, QC, Canada, Aug. 2020, pp. 1–5.
[30] N. Lu and Y. Zhang, "Design considerations of a centralized load controller using thermostatically controlled appliances for continuous regulation reserves," *IEEE Trans. Smart Grid*, vol. 4, no. 2, pp. 914–921, Jun. 2013.
[31] C. Wu, W. Gu, S. Zhou, and X. Chen, "Coordinated optimal power flow for integrated active distribution network and virtual power plants using decentralized algorithm," *IEEE Trans. Power Syst.*, early access, Jan. 5, 2021, doi: 10.1109/TPWRS.2021.3049418.
[32] L. Baringo and A. J. Conejo, "Strategic offering for a wind power producer," *IEEE Trans. Power Syst.*, vol. 28, no. 4, pp. 4645–4654, Nov. 2013.
[33] A. J. Conejo and C. Ruiz, "Complementarity, not optimization, is the language of markets," *IEEE Open Access J. Power Energy*, vol. 7, pp. 344–353, 2020.
[34] P. R. Hartley, K. B. Medlock, III, and O. Jankovska, "Electricity reform and retail pricing in Texas," *Energy Econ.*, vol. 80, pp. 1–11, May 2019.
[35] *Data Miner 2*, PJM, Audubon, PA, USA. Accessed: Mar. 16, 2021. [Online] Available: http://dataminer2.pjm.com/list
[36] F. Li, "Continuous locational marginal pricing (CLMP)," *IEEE Trans. Power Syst.*, vol. 22, no. 4, pp. 1638–1646, Nov. 2007.

Xiaofei Wang (Graduate Student Member, IEEE) received the B.S. degree from North China Electric Power University in 2014, and the M.S. degree from Wuhan University, China, in 2017. He is pursuing the Ph.D. degree with the University of Tennessee, Knoxville, USA. His research interests include distribution system optimization and demand response.

Fangxing (Fran) Li (Fellow, IEEE) received the B.S.E.E. and M.S.E.E. degrees from Southeast University, Nanjing, China, in 1994 and 1997, respectively, and the Ph.D. degree from Virginia Polytechnic Institute and State University, Blacksburg, VA, USA, in 2001. He is currently the James McConnell Professor with the University of Tennessee, Knoxville, TN, USA. His research interests include renewable energy integration, demand response, power markets, power system control, and power system computing. He is currently the Chair of IEEE Power System Operation, Planning and Economics Committee and the Editor-in-Chief of IEEE OPEN ACCESS JOURNAL OF POWER AND ENERGY.

Jin Dong (Member, IEEE) received the B.S. degree from the Harbin Institute of Technology, Harbin, China, in 2010, and the Ph.D. degree from the University of Tennessee, Knoxville, TN, USA, in 2016. He is currently a Research and Development Staff with the Grid Interactive Controls Group and with the Buildings Integration and Controls Research Group, Oak Ridge National Laboratory, Oak Ridge, TN, USA. His research interests lie in the intersection of smart buildings, building-to-grid integration, optimal control, and optimization.

Mohammed M. Olama (Senior Member, IEEE) received the B.S. and M.S. (Hons.) degrees in electrical engineering from the University of Jordan, Amman, Jordan, in 1998 and 2001, respectively, and the Ph.D. degree from the University of Tennessee, Knoxville, TN, USA, in 2007. He is currently a Senior Research Scientist with the Computational Sciences and Engineering Division, Oak Ridge National Laboratory, Oak Ridge, TN, USA. He is also an Adjunct Associate Professor with the EECS Department, University of Tennessee. His research interests include smart grid and smart buildings, smart grid communications and control, transactive control systems, and cyber–physical systems.

Qiwei Zhang (Graduate Student Member, IEEE) received the B.S.E.E. degree from North China Electrical Power University in 2016, and the M.S.E.E. degree from the University of Tennessee, Knoxville, in 2018, where he is currently pursuing the Ph.D. degree with the Department of Electrical Engineering and Computer Science. His research interests include cybersecurity in power systems, power system optimization, and market operation.

Qingxin Shi (Member, IEEE) received the B.S. degree from Zhejiang University, China, in 2011, the M.Sc. degree from the University of Alberta, Canada, in 2014, and the Ph.D. degree from the University of Tennessee, Knoxville, USA, in 2019, where he is working as a Research Assistant Professor. His research interests include demand response and distribution system resilience.

Byungkwon Park (Member, IEEE) received the B.S. degree in electrical engineering from Chonbuk National University, South Korea, in 2011, and the M.S. and Ph.D. degrees in electrical engineering from the University of Wisconsin–Madison, Madison, WI, USA, in 2014 and 2018, respectively. He is currently a Research Staff Member with the Computational Sciences and Engineering Division, Oak Ridge National Laboratory. His research interests include modeling, simulation, control, and optimization of electrical energy systems.

Teja Kuruganti (Senior Member, IEEE) received the M.S. and Ph.D. degrees in electrical engineering from the University of Tennessee, Knoxville, TN, USA, and the B.E. degree in electronics and communication engineering from Osmania University, Hyderabad, India. He is currently a Distinguished Research and Development Staff Member with Oak Ridge National Laboratory, Oak Ridge, TN, USA. His research interests include wireless sensor networks, modeling and simulation of communication and control systems, techniques for improving energy efficiency of buildings, and novel techniques for enabling grid-responsive building loads.